Probabilistic Localization and Mapping of Flexible Underwater Structures using Octomap

Bent Oddvar Arnesen[1], Stian Skaalvik Sandøy[1], Ingrid Schjølberg[1], Jo Arve Alfredsen[2], Ingrid Bouwer Utne[1]

***Abstract*— This paper addresses localization and mapping of flexible ocean structures. The methodology is based on a network of low cost acoustic transmitters on the structure and receivers stationed in the vicinity of the structure. The position of the receivers is assumed to be known. The position of each transmitter is estimated and represents a point position on the structure. All of the point positions are interpolated and applied in the mapping software Octomap, to build a digital map representation of the whole flexible structure. This map can serve as an environment model for underwater robots navigating close to such structures. An example is underwater robots operating close to or within a flexible ocean structure such as a fish cage.**

I. Introduction

Today, unmanned underwater vehicles (UUVs) are seeing increased use in underwater operations, especially in the oil and gas industry. Utilization of remotely operated underwater vehicles (ROVs) has also spread to the aquaculture industry [1]. Currently, the lack of robust navigation, guidance, control and planning regimes require human control of most of the vehicles' actions. Both perception of and self-localization within the environment are critical components for autonomous solutions in aquaculture [2], [3]. This paper presents a novel method for dynamic mapping of flexible underwater structures. The method uses acoustic telemetry transmitter tags and time synchronized hydrophones placed in a long baseline (LBL) network that receives the transmitter signals.

It is challenging to plan operations near flexible underwater structures when there is a lack of environmental information, and the representation of this information is therefore crucial. Octomap [4] is an open-source efficient mapping software that models a 3D world based on octrees. An illustration of how the software looks like is given in Figure 1, which shows a typical small size inspection class ROV within a fishcage. An octree stores a representation of a 3D world in a tree-based structure, where each parent node has eight child nodes. Each node in the tree represents a block (*voxel*) of the 3D world and each child node is a sub-voxel of its parent, thus giving higher resolution in the lower layers of the tree. The reasons for using Octomap are mainly based on its integration of measurement uncertainties in terms of probabilistic properties, modeling of unmapped areas and its high computational efficiency due to the internal architecture. It uses a grid based approach for mapping objects in 3D, where each grid cell has one property; a value between 0 and 1 that determines the probability of that a cell being occupied. Initially, Octomap generates an unknown environment as a 3D map, and updates the map by taking both sensor measurements and uncertainties of these measurements into account. The result is a digital map that is efficient in memory, that is possible to update, and that gives a realistic representation of the environment in which the robot will travel. Octomap is not used much for underwater applications, but it has been utilized to some extend, e.g., in [5] and [6].

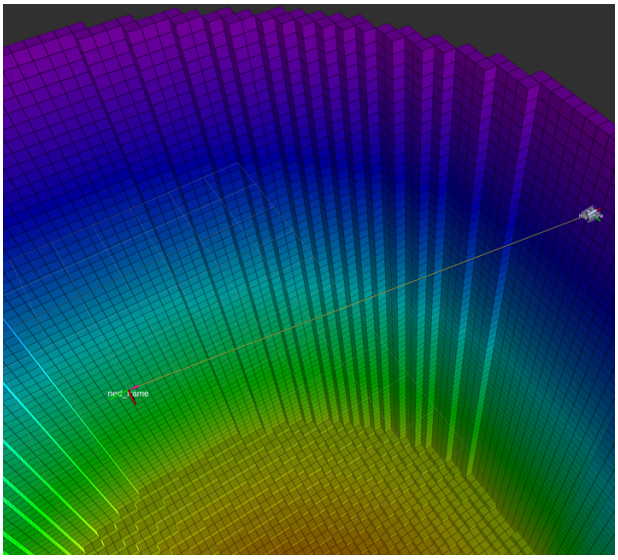

Fig. 1. An occupancy grid map of a fish cage in Octomap - A probabilistic 3D occupancy grid mapping software [4]. The digital map is a framework for visualization and a tool for achieving higher degrees of autonomy for robotic vehicles. The object to the left is the origin of a North-East-Down reference frame, and the object to the right is an underwater vehicle.

The use of acoustic-based positioning with transmitter tags and hydrophone receivers for a flexible structure has been conducted previously, e.g., [7] and [8]. However, the discussion of position estimate uncertainty is omitted. Transmitter tag position data are obtained by adopting the time difference of arrival (TDOA) method [9], [10]. This technique calculates the position of a transmitter based on the signal TDOA at multiple receivers at different, but known locations and the velocity of the signal. The map of a structure can be produced by interpolating tag positions in smart ways, which in turn can be used for visualization purposes or be part of a digital map aiding in robotic vehicle navigation.

[1]Department of Marine Technology, Norwegian University of Science and Technology, Otto Nielsens Vei 10, 7052 Trondheim, Norway
{bent.o.arnesen, stian.s.sandoy, ingrid.schjolberg, ingrid.b.utne }@ntnu.no

[2]Department of Engineering Cybernetics, Norwegian University of Science and Technology, Høgskoleringen 1, 7043 Trondheim, Norway
jo.arve.alfredsen@ntnu.no

Keeping track of where the vehicle is and where it is going is necessary in order to perform path-following and trajectory tracking for underwater vehicles [11], [12], or to perform intervention operations where the location of certain objects and structures are of importance [13].

A. Problem Description

This paper is concerned with estimating the position of a flexible structure that is located below the sea surface. A set of transmitter tags are distributed over a structure in key locations. The tags send signals that are received by hydrophones stationed just below the surface. The location of the structure is mapped by estimating the position of the tags, and interpolating between these. Measurement and estimation uncertainties are combined in a mapping software named Octomap for visualization of a probability based occupancy grid map in 3D space.

B. Contribution

The contribution of this paper is a method for estimating the position of a flexible structure below the sea surface. The structure is plotted in a digital map in the software Octomap. This map can serve as a tool for robotic vehicles that seek to plan and execute operations autonomously within and around the structure and for visualization purposes.

II. Instrumentation

The presented work is based on the TBR700-RT digital hydrophone receivers [14] and acoustic transmitter tags of type ADT-HP16 [15] (Thelma Biotel AS, Trondheim, Norway). The equipment is normally used as a fisheries research tool for remote monitoring of the position, behavior and health of fish. Information is transmitted by the tags regularly using acoustic telemetry. The hydrophones are time synchronized through a surface synchronization module (SSM) by utilizing global navigation satellite system (GNSS) signals. By placing a hydrophone directly beneath an SSM at a known depth, the SSM provides estimates of the hydrophone's position.

Table I contains the specification of the equipment, while Figure 2 gives an overview of the hardware setup. The telemetry tags transmit a modulated acoustic signal containing the unique tag id number and hydrostatic pressure. When the signal is received, it is given a time stamp by the hydrophones, which again are time synchronized by the SSMs.

III. Preliminaries and Notation

A. Reference Frame

In this work, the North-East-Down (NED) reference frame has been chosen to represent position estimates below the sea surface, while the remaining position estimates uses the global navigation satelite system (GNSS) in an Earth-centered-Earth-fixed (ECEF) reference frame. More information about reference frames and how they relate to each other can be found in [17].

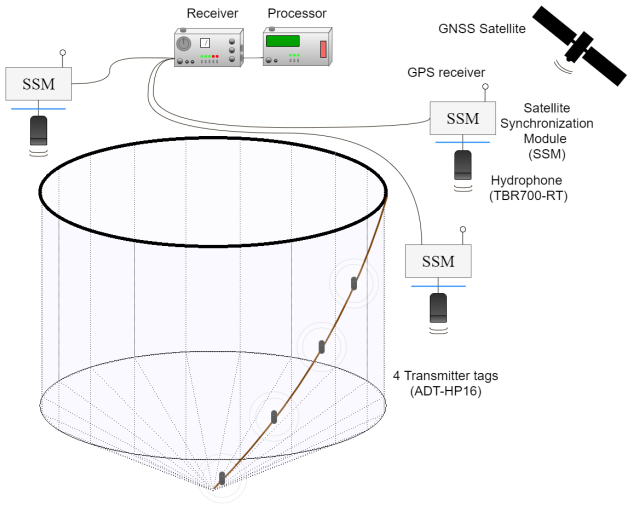

Fig. 2. Conceptual description of equipment setup and signal flow. Transmitter tag signals are received by a network of hydrophones with position updates from GNSS satellites. Tag signals are time synchronized by the SSMs, before they are forwarded to a receiver and a processor to estimate the position of the transmitter tags.

TABLE I
Instrumentation Specification

ADT-HP16	
Size	Length x Diameter = 70 mm x 15 mm
Weight	15 g in water, 29 g in air
Signal Strength	157-160 dB
Transmit Frequency	Transmit every 60 s
Battry Life	2-3 years
Operating Freq.	69 kHz
Data	Pressure, Tag-ID
TBR700-RT with SSM	
Size	Length x Diameter = 230 mm x 75 mm
Weight	0.26 kg in water, 1.14 kg in air
Operating Freq.	60-80 kHz
Interface	USB, Bluetooth, RS-485
Data Storage	1.5 million detections
Battery Life	8-9 Months
Time stamp resolution	milliseconds
SSM	
GNSS Module	NEO-7P [16]
Data	Synchronized time, Position fix

B. Underwater Acoustics

Electromagnetic waves from GNSS signals, such as the Global Positioning System (GPS), can be used to estimate the position of objects. However, this only works above the sea surface, due to strong subsurface attenuation of electromagnetic waves. On the other hand, sound waves (acoustics) are pressure differences/oscillations generated by mechanical vibrations. These vibrations can be modulated to transmit data, and subsequently demodulated to extract the data. The speed of the wave propagation is determined by the properties of the medium in which it travels. For sea water, sound velocity can be represented by the empirical formula [18]

$$\begin{aligned} c =& 1448.6 + 4.6418T - 0.0523T^2 \\ &+ 1.25(S-35) + 0.017D, \end{aligned} \tag{1}$$

where T, S, c, D corresponds to temperature [$^\circ C$], salinity

[‰], speed of sound $[m/s]$ and depth $[m]$, respectively. Sound speed gradients lead to bending effects of the sound wave [19]. Sound intensity is usually measured in decibel, with a reference to a sound pressure level (the pressure induced by the sound wave) of $1\mu Pa$ (or [dB re 1μPa]). The formula is given as:

$$dB = 20\log_{10}\left(\frac{p^d}{p_0^d}\right), \tag{2}$$

where p^d is the root mean square (RMS) pressure and p_0^d is a reference pressure.

C. Received Signal Strength

The signal to noise ratio (SNR) describes the received signal strength (RSS) relative to the average background noise [18]:

$$SNR = 20\log_{10}\left(\frac{\text{Average peak signal amplitude}}{\text{Average noise amplitude}}\right) \tag{3}$$

The average peak signal amplitude can be viewed as the RSS, while the average noise amplitude is the variance of the RSS signal, provided by the receivers. As can be seen from (3), the SNR is higher the closer the source is to the receiver. The signal strength decreases with range, mainly due to absorption and geometrical spreading loss. Absorption is due to energy loss to the environment and depends on many variables, such as temperature, wave frequency, salinity, pH level and depth. Geometrical spreading occurs because of the increased area over which the sound energy is distributed as the wave propagates. The received signal strength (RSS) is dependent on the distance from the source, and can be formulated according to [20] as the following equation

$$RSS\ (r) = SL_0 - \alpha(r - r_0) - 20log\left(\frac{r}{r_0}\right) + \epsilon_{RSS}, \tag{4}$$

where r is the distance from the source, r_0 is the reference distance where the signal strength is measured, α is the absorption coefficient and ϵ_{RSS} is the Gaussian white noise of the signal. Furthermore, SL_0 represents the source level at the reference distance. The distance r, which is given as $r = ||p - p_i||$, represents the distance between a tag position p and a hydrophone position p_i. By inserting $r = ||p - p_i||$ into (4) and setting the reference distance $r_0 = 1$, the RSS measurement equation for hydrophone no. i for a given tag is obtained as

$$RSS_i\ (r) = SL_0 - (||p - p_i|| - 1)\alpha - 20log(||p - p_i||) + \epsilon_{RSS_i} \tag{5}$$

D. Time Difference of Arrival

The time difference of arrival (TDOA) at different receiver locations can be utilized to determine the position of the source of a transmitted signal, given that the positions of the signal receivers are known [9], [20], [21]. A sound signal is sent from a transmitter tag in position p, and received at locations p_i at time t_i for receiver number $i = 1, 2, 3$, where t_i is calculated as

$$t_i = \frac{||p - p_i||}{c_0} \quad i = 1, 2, 3 \tag{6}$$

Note that (6) is an approximation, since the speed of sound generally will vary depending on the properties of water between transmitter and receiver (see (1)). Choosing the sound speed to be constant is a reasonable approximation over short distances. From (6), an expression estimating the TDOA between a receiver at position i and j can be obtained as

$$dt_{ij} = \frac{1}{c_0}(||p - p_i|| - ||p - p_j||) + \epsilon_{dt_i} - \epsilon_{dt_j} \tag{7}$$

The term dt_{ij} is the time-difference between a signal that was received at receiver i and j. Furthermore, ϵ_{dt_i} and ϵ_{dt_j} represents Gaussian white noise. These terms incorporate errors, such as timing errors due to clock drift, limitations on synchronization accuracy, or limitations in resolution on the time stamp, bending effects of the sound wave, and so forth.

E. Depth - Pressure Measurement

The static pressure measurement made locally by the transmitter tag is highly valuable, as it can be used to determine its depth with centimeter accuracy, and is given by equation

$$P_m = \rho g z + P_s + \rho g \epsilon_z \tag{8}$$

The depth measured from the surface is given by z, where P_m is pressure measured by the pressure sensor, P_s is the pressure at the surface corresponding to 1 atm, ρ is the density of sea water, g is the gravitational constant and ϵ_z is pressure sensor measurement noise.

IV. Position Estimator

To estimate the transmitter tag positions based on TDOA measurements, RSS data and depth measurements, an extended Kalman filter (EKF) was implemented to fuse the available sensor measurements together in a probabilistic manner, in line with [22]. The filter assumes that all noise terms are independent of each other. The discrete process and measurement model for estimating the TDOA is designed as

$$p_{k+1} = p_k + \epsilon_{p_{1:3}} \tag{9}$$

$$y_k = h(p_k, p_i, \epsilon) \tag{10}$$

where p_k, $p_{k+1} \in \mathbf{R}^{3\times1}$ are state vectors at time instants k and $k + 1$, respectively, containing the North, East and Down position. The random variable $\epsilon_{p_{1:3}} \in \mathbf{R}^{3\times1}$ is Gaussian distributed noise by $N(0, Q)$, where $Q \in \mathbf{R}^{3\times3}$ is the covariance matrix of the probability distribution. This model is also known as a random walk process, which is used to model slowly varying processes [23]. Furthermore, $y_k \in \mathbf{R}^{2m\times1}$ in (10) is the measurement vector at time instant k, where m is the number of signal receivers. The measurements can

be described by the nonlinear function $h(p_k, p_i, \epsilon) \in \mathbf{R}^{2m\times 1}$, where p_i is a random variable of the receiver position with a distribution N(0,$\Sigma^2_{p_i}$), where $i = 1, \ldots, m$ denotes the signal receiver number. The parameter $\Sigma^2_{p_i} \in \mathbf{R}^{3\times 3}$ represents the uncertainty of the receiver position, and $\epsilon = \{\epsilon_{dt_i}, \epsilon_{RSS_i}, \epsilon_z\}$ corresponds to the random variable noise terms in (5), (7) and (8). Based on the measurement in (5), (7) and (8), y_k in (10) is found as

$$\underbrace{\begin{bmatrix} dt_{12} \\ \vdots \\ dt_{(m-1)m} \\ RSS_1 \\ \vdots \\ RSS_m \\ \frac{(P_m - P_s)}{\rho g} \end{bmatrix}}_{y_k} = \underbrace{\begin{bmatrix} \frac{1}{c_0}(\ (r_1 - r_2) + \epsilon_{dt_1} - \epsilon_{dt_2}) \\ \vdots \\ \frac{1}{c_0}(\ (r_{m-1} - r_m) + \epsilon_{dt_{m-1}} - \epsilon_{dt_m}) \\ SL_0 - 20\log(r_1) - \alpha(r_1 - 1) + \epsilon_{RSS_1} \\ \vdots \\ SL_0 - 20\log(r_m) - \alpha(r_m - 1) + \epsilon_{RSS_m} \\ z + \epsilon_z \end{bmatrix}}_{h(p_k, p_i, \epsilon)} \tag{11}$$

where r is the distance from the source, as before, now re-defined as $r_i = ||p_k - p_i||$.

A. Covariance and Measurement Model Linearization

The function $h(p_k, p_i, \epsilon)$ is nonlinear, and cannot be used directly in an EKF. Therefore, it is necessary to linearize the measurement matrix and the covariance matrix. These can be linearized with the position predicted by the filter, i.e., $\bar{p}_k$. The linearization of of the covariance matrix R_k at each time step k can be approximated with a Taylor expansion [24], given as

$$R_k = Var(h(p_i, \epsilon)) \approx S_k \Sigma^2 S_k^T, \tag{12}$$

where $S_k = \frac{\partial h(p, p_i, \epsilon)}{\partial\{\epsilon, p_i\}}|_{p_k = \bar{p}_k} \in \mathbf{R}^{2m\times(5m+1)}$ is the Jacobian of (11), computed as

$$S_k = \begin{bmatrix} \frac{\partial h_1}{\partial \epsilon p_{1:m}} & & \frac{\partial h_1}{\partial \epsilon_{dt_{1:m}}} & 0 \cdots 0 & 0 \\ \vdots & & \vdots & \vdots \cdots \vdots & \vdots \\ \frac{\partial h_{m-1}}{\partial \epsilon p_{1:m}} & & \frac{\partial h_{m-1}}{\partial \epsilon_{dt_{1:m}}} & 0 \cdots 0 & 0 \\ \frac{\partial h_m}{\partial \epsilon p_{1:m}} & 0 \cdots 0 & & \frac{\partial h_m}{\partial \epsilon_{RSS_{1:m}}} & 0 \\ \vdots & \vdots \cdots \vdots & & \vdots & \vdots \\ \frac{\partial h_{2m-1}}{\partial \epsilon p_{1:m}} & 0 \cdots 0 & & \frac{\partial h_{2m-1}}{\partial \epsilon_{RSS_{1:m}}} & 0 \\ 0 \cdots 0 & 0 \cdots 0 & & 0 \cdots 0 & \frac{\partial h_{2m}}{\partial \epsilon_z} \end{bmatrix} \tag{13}$$

where the calculations of the derivatives are given in the Appendix. Σ^2 is the covariance matrix given by

$$\Sigma^2 = diag(\Sigma^2_{p_1}, \ldots, \Sigma^2_{p_m}, \sigma^2_{dt_1}, \ldots, \sigma^2_{dt_m}, \sigma^2_{RSS_1}, \ldots, \sigma^2_{RSS_m}, \sigma^2_z) \in \mathbf{R}^{5m+1\times 5m+1} \tag{14}$$

The parameter $\Sigma_{p_i} = diag(\sigma_{p_1}, \sigma_{p_2}, \sigma_{p_3})$ denotes the covariance matrix for the position of receiver no. i, obtained by the accuracy of the calibration procedure of the receivers. $\sigma^2_{dt_i} \in \mathbf{R}$ denotes variance on the time stamp for each receiver, $\sigma^2_{RSS_i} \in \mathbf{R}$ is the noise on the estimated RSS and $\sigma^2_z \in \mathbf{R}$ represents noise from the pressure sensor. Moving on with the linearization procedure, the linearized measurement matrix C_k is obtained by taking the Jacobian of (11) as follows

$$\begin{aligned} C_k &= \frac{\partial h(p_k, p_i, \epsilon)}{\partial p_k}|_{p_k = \bar{p}_k} \\ &= \begin{bmatrix} \frac{1}{c_0}(\frac{(p_k - p_1)^T}{r_1} - \frac{(p_k - p_2)^T}{r_2}) \\ \vdots \\ \frac{1}{c_0}(\frac{(p_k - p_{m-1})^T}{r_{m-1}} - \frac{(p_k - p_m)^T}{r_m}) \\ -\alpha\frac{(p_k - p_1)^T}{r_1} - \frac{20(p - p_1)^T}{r_1^2 \ln(10)} \\ \vdots \\ -\alpha\frac{(p - p_m)^T}{r_m} - \frac{20(p - p_m)^T}{r_m^2 \ln(10)} \\ 0 \quad 0 \quad 1 \end{bmatrix}_{p_k = \bar{p}_k} \end{aligned} \tag{15}$$

The algorithm applied for estimating the transmitter source and receiver positions can be found in Algorithm 1. Here, $Q \in \mathbf{R}^{3\times 3}$ and $R_k \in \mathbf{R}^{2m\times 2m}$ are the process and measurement covariance matrices, respectively, where m is the number of hydrophones. K_k is the Kalman gain and $\hat{P}_k$ is the estimated covariance matrix.

Data: Intial estimate $\bar{p}_0$, Init Covariance matrix $\bar{P}_0$,
Result: Tag position, Tag position uncertainty
if *Measurement* y_k *Received* **then**

$$\begin{aligned} R_k &= S_k \Sigma^2 S_k^T \\ C_k &= \frac{\partial h(p_k, p_i, \epsilon)}{\partial p_k}|_{p_k = \bar{p}_k} \\ K_k &= \bar{P}_k C_k^T (C_k \bar{P} C_k^T + R_k)^{-1} \\ \hat{p}_k &= \bar{p}_k + K_k(y_k - h(\bar{p}_k)) \\ \hat{P}_k &= (I_{3\times 3} - K_k C_k)\bar{P}_k (I_{3\times 3} - K_k C_k)^T + K_k R_k K_k^T \\ \bar{p}_{k+1} &= \hat{p}_k \\ \bar{P}_{k+1} &= \hat{P}_k + Q \end{aligned}$$

end

Algorithm 1: EKF algorithm

V. Case Study: Position of an Anchor Line Numerical Simulations

This section presents a case study where the goal is to estimate the position of a rope / anchor line, which represents a typical flexible underwater structure. A numerical simulation study is conducted in a static environment with three hydrophones (receivers) and four transmitter tags distributed over the rope. First, transmitter tag positions are estimated, before they are interpolated in order to map the position of the anchor line. The estimated uncertainties are incorporated in the position estimates based on the covariance matrix from the EKF as confidence intervals in 3D space. Numerical simulations are based on a static data set with noises and

uncertainties that aim to replicate uncertainties encountered in the real world, as presented in Sections II-III.

A. Structure Modelling: Anchor Line

In this subsection, the modelling technique of the anchor line is studied. An initial assumption about the anchor line is made:

Assumption 1: The anchor line can be assumed to be fully stretched between two neighboring tags.

Two neighboring points (tag positions) are marked on the line, $p_0 = \begin{bmatrix} x_0 & y_0 & z_0 \end{bmatrix}^T$ and $p_1 = \begin{bmatrix} x_1 & y_1 & z_1 \end{bmatrix}^T$. Due to Assumption 1, a straight-line parametrization s can be parametrized by a variable t as $s(t) = A(t)x,\ s(t) \in \mathbf{R}^3$. By letting the parameterization variable t run between 0 and 1, $A(t)$ and x can be defined as

$$A = \begin{bmatrix} (1-t) & 0 & 0 & t & 0 & 0 \\ 0 & (1-t) & 0 & 0 & t & 0 \\ 0 & 0 & (1-t) & 0 & 0 & t \end{bmatrix} \tag{16}$$

$$x = \begin{bmatrix} x_0 & y_0 & z_0 & x_1 & y_1 & z_1 \end{bmatrix}^T \tag{17}$$

B. Confidence Interval Representation

The uncertainty of a position estimate needs to be incorporated with the position estimates, as estimates cannot be guaranteed to be correct. One way to merge uncertainties and position estimates is to make use of the covariance matrix from the EKF. Therefore, a second assumption is made:

Assumption 2: The covariance matrix calculated by the EKF can be used to describe the confidence interval of tag position estimates.

The covariance of the parametrization is estimated by the EKF, and is given as $\Sigma_0,\ \Sigma_1 \in \mathbf{R}^{3\times3}$ for $p_0,\ p_1$, respectively. The confidence interval provides a range of values that are likely to contain the population parameter of interest. These are specified as confidence interval levels. For instance, a 95% confidence interval may be chosen. This means that if the same population is sampled on an infinite number of occasions with the same confidence level, the resulting interval would contain the population parameter in exactly 95% of the cases. By Assumptions 1-2, the covariance matrix *covar* if found as a function of the parametrization $s(t)$ as

$$covar(s(t)) = A\Sigma_c A^T \in \mathbf{R}^{3\times3} \tag{18}$$

where

$$\Sigma_c = \begin{bmatrix} \Sigma_0 & 0 \\ 0 & \Sigma_1 \end{bmatrix} \in \mathbf{R}^{6\times6} \tag{19}$$

Theoretically, the confidence interval is a sphere for Gaussian distributed errors in 3D space, but now becomes an ellipsoid with the covariance values being non-zero. Before moving on, an assumption about the depth measurements is made.

Assumption 3: Assume that the pressure sensor uncertainty is so small that it can be neglected. It then follows that the depth position estimate by the EKF is the true depth.

According to Assumption 3, the confidence interval is reduced from an ellipsoid in 3D to an ellipse in 2D in the North-East plane. In order to calculate the error covariance ellipse, the covariance matrix $covar(s(t))$ and a 95% confidence interval is chosen. Ideally, a short interval with a high degree of confidence is desired, which is why the 95% confidence interval usually is chosen [24]. Both the method and a proof of the method presented here can be found in [25]. The confidence interval is obtained by assuming a multivariate Gaussian distributed data set with zero covariance, which means that North and East position data are normally distributed. The ellipse can be calculated as

$$\left(\frac{x}{\sigma_x}\right)^2 + \left(\frac{y}{\sigma_y}\right)^2 = \sigma_s, \tag{20}$$

where σ_s is the scale of the ellipse, i.e., the confidence interval value. The sum is distributed by a χ^2-distribution, and for the 95% confidence interval, the scale is found as $\sigma_s = 5.99$ (p. 760 in [25]). The ellipse is easily obtained based on the scale σ_s and the estimated North- and East values from the EKF at any desired depth.

C. Results

The EKF is given an initial tag position $\bar{p}_0 = \begin{bmatrix} 0 & 0 & 5 \end{bmatrix}^T$ and covariance matrix $\bar{P}_0 = 25^2 \cdot I_{3\times3}$. Variance terms are chosen as $\Sigma^2_{p_i} = \text{diag}(1^2, 1^2, 0.02^2)$ on the hydrophone position, $\sigma^2_{dt_i} = (5 \cdot 10^{-4})^2$ on the time stamp and $\sigma^2_{RSS_i} = 10^2$ on the RSS signal for all hydrophones. Furthermore, the variance $\sigma^2_{p_j} = 0.01^2$ is applied on the tag positions for tag no. $j = 1, 2, 3, 4$, and $\sigma^2_z = 0.02^2$ on the depth sensor readings. The remaining parameters used in the case study can be found in Table II. It should be noted that the sound speed c_0 is calculated as in (1), the source level at reference distance SL_0 is used to estimate RSS in (5), and the absorption coefficient α is found based on the work of [19], using the wave frequency ω_{wf}, temperature T and salinity S in Table II.

TABLE II
SIMULATION PARAMETERS

Description	Parameter	Value
Temperature	T	13 [°C]
Salinity	S	35 [‰]
Depth	D	7.5 [m]
Sound velocity	c_0	1500 $[\frac{m}{s}]$
Gravitational constant	g	9.81 $[\frac{kg\,m}{s^2}]$
Sea water density	ρ	1025 $[\frac{kg}{m^3}]$
Source level at reference distance	SL_0	160 [dB]
Absorption coefficient	α	$21.9{\cdot}10^{-4}[\frac{dB}{m}]$
Wave frequency	ω_{wf}	69 [kHz]

Running 3000 Monte Carlo simulations with these parameters gives the average of the root mean square errors (RMSE). In RMSE_1, RSS measurements are used, while these are not included in RMSE_2. The results can be found in Table III. One simulation with RSS measurements are shown with the covariance error ellipse representation in Figure 3.

TABLE III

INITIALIZATION PARAMETERS AND RMSE FOR EACH TAG AFTER 3000 MONTE CARLO SIMULATIONS.

Tag no.	**1**	**2**	**3**	**4**
$\bar{p}_0$	(0,0,5)	(0,0,5)	(0,0,5)	(0,0,5)
True Position	(5,-5,5)	(7.5,-7.5,10)	(10,-10,15)	(15,-15,25)
$RMSE_1$ [m]	0.173	0.219	0.270	0.448
$RMSE_2$ [m]	0.175	0.220	0.271	0.449
Hydrophone	**p_1**	**p_2**	**p_3**	
Position	(0,0,0)	(15,0,0)	(0,-15,0)	

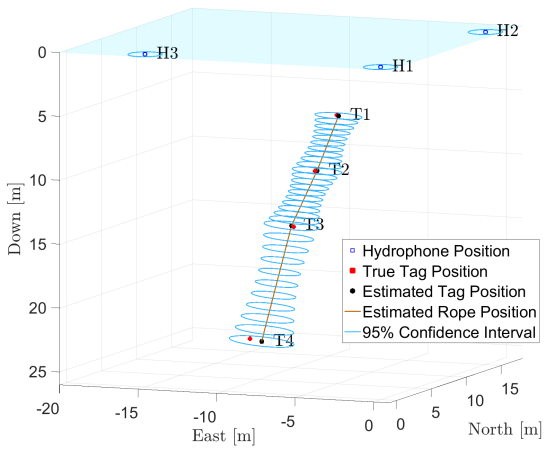

Fig. 3. This figure shows the hydrophone and tag positions with corresponding confidence error ellipses after 60 minutes. The blue and black squares represent the hydrophone and tag positions, respectively. The blue ellipses correspond to the 95% confidence interval in the North-East plane for the hydrophone and tag positions. H1, H2 and H3 represent hydrophone no. 1, 2 and 3, while T1, T2, T3 and T4 represent tag no. 1, 2, 3 and 4, respectively.

By Assumptions 1-3, the interpolation method from Section V-A is applied to create the occupancy grid map. All depth intervals are equally spaced by 10 cm, each containing a Gaussian distributed 2D point cloud based on the mean and the covariance matrix from the EKF. The resulting map with anchor line position and uncertainties can be seen as an occupancy grid map in Figure 4.

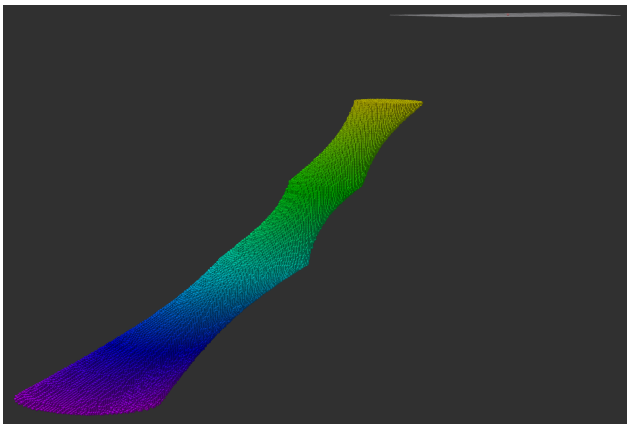

Fig. 4. An occupancy grid map of the anchor line in Octomap. The structure is drawn as a set of 3D grid cells based on a point cloud, generated within the confidence interval boundaries.

Perhaps more interestingly, the estimation process and convergence towards the true tag positions for the tag closest to and furthest away from the surface are illustrated in Figures 5 and 6, respectively. For tag no. 1, the position estimate converges after less than five minutes (five measurements, one measurement every minute), while convergence for tag no. 4 takes approximately 40 minutes.

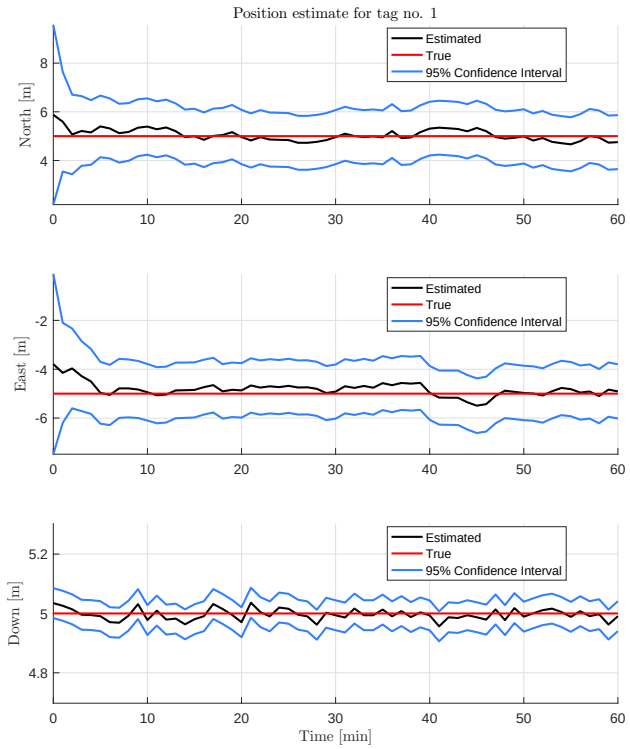

Fig. 5. True tag position (red) vs. estimated tag position (black) for tag no. 1 (T1). The blue lines represent the 95% confidence interval

VI. DISCUSSION

This section discusses the validity of the assumptions and the methods used to estimate the tag positions.

The data set of which the numerical simulation case study is based upon is static for 60 minutes, meaning that all values are constant for the entire case study. This is not realistic, not even in calm sea states, where slowly varying fluctuations such as currents do exist. Therefore, noise is included in the model based on the environment and the equipment measurement inaccuracies. The time stamp on the received signal is the main contributor to errors in the position estimates, which has a millisecond resolution. By assuming that the typical sound speed in water is 1500 m/s, a millisecond resolution implies that the position data may have an error up to $1500[m/s] \cdot 0.001[s] = 1.5[m]$. Though, with enough measurements, the RMS error can go below 1.5m. The RSS data are range measurements, but these values can be unreliable due to, e.g., the direction in which the hydrophone points or due to a non-spherical wave front. This is why the measurement noise σ_{RSS} is set high, and based on the RMSE data presented in Table III, it can be seen

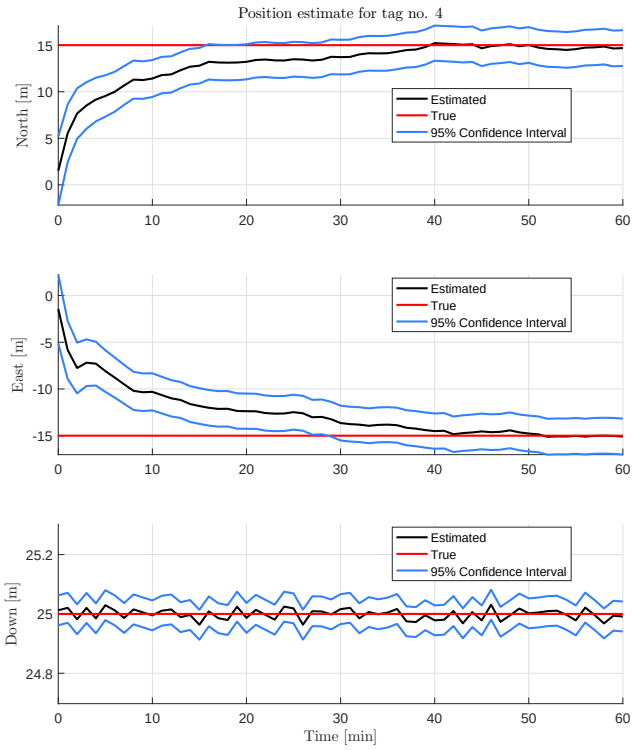

Fig. 6. True tag position (red) vs. estimated tag position (black) for tag no. 4 (T4). The blue lines represent the 95% confidence interval

that the inclusion of RSS measurements only has a marginal improvement for all tag position estimates, which may be due to the large values for σ_{RSS} and SL_0. Nevertheless, the RSS measurements can be valuable when fused with other measurements, depending on the signal quality.

The convergence rate and estimation accuracy are heavily dependent on each tag's position relative to the receiver network geometry, which is known as the dilution of precision (DOP). Poor DOP areas are nonlinear, where even the smallest measurement errors can lead to large estimation errors, mainly caused by a non-Gaussian distribution and lost information about the system in the linearization phase. To avoid this, another filter could be implemented, e.g., a particle filter (PF) or an unscended Kalman filter (UKF). These estimators do not require linearization and are better suited to describe non-Gaussian distributions. However, if the hydrophones are strategically placed according to the tag positions, the EKF should match the performance of a PF and UKF, especially if there is little noise on the measurements, given that the nonlinearities are sufficiently reduced. It should be noted that motions on the hydrophones due to waves and currents can affect the transmitter position estimates. These disturbances may, for instance, be filtered out by utilizing the method developed in [26].

When considering the hardware, designing the receivers to have microsecond time stamp resolution would highly improve the final accuracy in the estimate. Other error sources are due to the tuning of variances. The GPS positions for the hydrophones are estimated to have a variance of $\Sigma_p = 1m$ in the horizontal plane, which might be a bit high, as RTK dGPS (real-time kinematic differential GPS) or precise point positioning (PPP) can give error estimates below $1m$. Moreover, a decent pressure sensor should give depth errors below $5cm$, which is the main motivation for letting the confidence intervals describe confidence error ellipses instead of ellipsoids.

In this case study, only four tags were used, while in a fish cage, it may be necessary to have several more to accurately model the structure. As an example, consider the following: If it is known that environmental forces are small, the cage will be almost perfectly cylindrical. Since each of the tags represent a point position on the structure, it would be sufficient with 3 tags to accurately model a perfectly cylindrical cage at a given depth, where the interpolation strategy would be to draw a circle that intersects the given tag point positions. However, the assumption that the cage is perfectly cylindrical may not be valid in a real life scenario, and it is highly likely that more tags will be needed to accurately model the cage structure. Not only does the accuracy of the model depend on the number of tags used, but also the properties of the water, the environmental forces and the structure, accuracy of position estimates, noises and noise distributions, delays and processing time, DOP and the interpolation strategy.

Greater accuracy of the underwater tag position estimates can be achieved by customizing tags for higher update rates and with larger batteries. Combining this with sensor technologies such as doppler velocity loggers (DVLs), sonars and cameras on an underwater vehicle can give additional updates of the position of objects in the map, and may increase the positioning accuracy. A digital map that incorporates a strategy for handling inaccuracies and that can be used for navigation purposes has the potential to increase the autonomy level in underwater vehicles performing operations in offshore and aquaculture industry.

VII. Conclusions

In this paper, a method for estimating the position of acoustic transmitter tags on a flexible structure, represented by an anchor line, has been developed. The interpolation strategy is applied in a numerical simulation case study with good results. The simulation study showed that the position of the anchor line is estimated with less than 0.5m error. The position data were given as input to Octomap, to generate a probabilistic 3D occupancy grid map. However, the error estimates can be significantly reduced through improved calibration procedures. This work shows that there is an immense potential to improve underwater positioning of flexible structures using position information in a probabilistic occupancy grid map. By utilizing Octomap and estimating confidence intervals for the measurements and filter estimations, it is expected that this map could give a sufficient representation of the ocean structure. Such a probabilistic representation of the environment is important for underwater vehicles operating close to or within the structure, and may lay a foundation for increased level of autonomy in inspection, maintenance and repair operations. Customizing point tags

for higher update rates and with larger batteries, where weight and size are not limiting factors, position estimates will be improved. Sensor information from, e.g., doppler velocity loggers (DVLs), sonars and cameras on the vehicle can be applied to update the geometrical representation of the underwater environment. A digital map, such as the Octomap, can both be used as a visualization tool for ROV operators and supervisory tasks, and as a framework for underwater vehicles to enhance their autonomous capabilities through improved planning, guidance, navigation and control strategies.

Acknowledgment

This work is funded by the Norwegian University of Science and Technology (NTNU), Norwegian Research Council projects Reducing Risk in Aquaculture (254913) and SFI Exposed (237790).

Appendix

$$
\begin{aligned}
\frac{\partial h_i}{\partial \epsilon_{p_i}} &= \frac{(p_k - p_i)^T}{c_0 r_i} \\
\frac{\partial h_i}{\partial \epsilon_{p_j}} &= \begin{bmatrix} 0 & 0 & 0 \end{bmatrix}, \quad j \neq i \\
\frac{\partial h_1}{\partial \epsilon_{dt_{1:m}}} &= \begin{bmatrix} 1 & 1 & 0 & \cdots & 0 \end{bmatrix} \in \mathbf{R}^{1\times m} \\
\frac{\partial h_2}{\partial \epsilon_{dt_{1:m}}} &= \begin{bmatrix} 0 & 1 & 1 & 0 & \cdots & 0 \end{bmatrix} \in \mathbf{R}^{1\times m} \\
\frac{\partial h_{m-1}}{\partial \epsilon_{dt_{1:m}}} &= \begin{bmatrix} 0 & \cdots & 0 & 1 & 1 \end{bmatrix} \in \mathbf{R}^{1\times m} \\
\frac{\partial h_m}{\partial \epsilon_{RSS_{1:m}}} &= \begin{bmatrix} 1 & 0 & \cdots & 0 \end{bmatrix} \in \mathbf{R}^{1\times m} \\
\frac{\partial h_{2m-1}}{\partial \epsilon_{RSS_{1:m}}} &= \begin{bmatrix} 0 & \cdots & 0 & 1 \end{bmatrix} \in \mathbf{R}^{1\times m} \\
\frac{\partial h_{2m}}{\partial \epsilon_z} &= 1
\end{aligned}
$$

References

[1] M. Føre, K. Frank, T. Norton, E. Svendsen, J. A. Alfredsen, T. Dempster, H. Eguiraun, W. Watson, A. Stahl, L. M. Sunde, C. Schellewald, K. R. Skøien, M. O. Alver, and D. Berckmans, "Precision fish farming: A new framework to improve production in aquaculture," *Biosystems Engineering*, 2017.

[2] I. Schjølberg, T. B. Gjersvik, A. A. Transeth, and I. B. Utne, "Next generation subsea inspection, maintenance and repair operations," *IFAC-PapersOnLine*, vol. 49, no. 23, pp. 434–439, 2016.

[3] I. Schjølberg and I. B. Utne, "Towards autonomy in rov operations," *IFAC-PapersOnLine*, vol. 48, no. 2, pp. 183–188, 2015.

[4] A. Hornung, K. M. Wurm, M. Bennewitz, C. Stachniss, and W. Burgard, "OctoMap: an efficient probabilistic 3D mapping framework based on octrees," *Autonomous Robots*, vol. 34, pp. 189–206, 2013.

[5] G. Vallicrosa, A. Palomer, D. Ribas, and P. Ridao, *Realtime AUV Terrain Based Navigation with Octomap in a Natural Environment*. Cham: Springer International Publishing, 2014, pp. 41–53.

[6] J. D. HernÃąndez, K. IsteniÄŊ, N. Gracias, N. Palomeras, R. Campos, E. Vidal, R. GarcÃŋa, and M. Carreras, "Autonomous underwater navigation and optical mapping in unknown natural environments," *Sensors (Basel, Switzerland)*, vol. 16, no. 8, p. 1174, 2016.

[7] P. Klebert, y. Patursson, P. C. Endresen, P. Rundtop, J. Birkevold, and H. W. Rasmussen, "Three-dimensional deformation of a large circular flexible sea cage in high currents: Field experiment and modeling," *Ocean Engineering*, vol. 104, pp. 511–520, 2015.

[8] J. DeCew, D. W. Fredriksson, P. F. Lader, M. Chambers, W. H. Howell, M. Osienki, B. Celikkol, K. Frank, and E. Høy, "Field measurements of cage deformation using acoustic sensors," *Aquacultural Engineering*, vol. 57, pp. 114–125, 2013.

[9] F. Gustafsson and F. Gunnarsson, "Positioning using time-difference of arrival measurements," in *Acoustics, Speech, and Signal Processing, 2003. Proceedings. (ICASSP '03). 2003 IEEE International Conference on*, vol. 6, April 2003, pp. VI–553–6 vol.6.

[10] C. Rascon and I. Meza, "Localization of sound sources in robotics: A review," *Robotics and Autonomous Systems*, vol. 96, pp. 184–210, 2017.

[11] B. O. Arnesen, A. M. Lekkas, and I. Schjølberg, "3D Path Following and Tracking for an Inspection Class ROV," no. 57731, 2017. [Online]. Available: http://dx.doi.org/10.1115/OMAE2017-61170

[12] D. J. W. Belleter, C. Paliotta, M. Maggiore, and K. Y. Pettersen, "Path following for underactuated marine vessels," *IFAC-PapersOnLine*, vol. 49, no. 18, pp. 588–593, 2016.

[13] M. Jacobi, "Autonomous inspection of underwater structures," *Robotics and Autonomous Systems*, vol. 67, pp. 80–86, 2015.

[14] ThelmaBiotel, "TBR-700 REALTIME," http://www.thelmabiotel.com/index.php?pageId=580, [Accessed: 22.08.2017].

[15] ThelmaBiotel, "ID tag 16mm," http://www.thelmabiotel.com/index.php?pageId=567 [Accessed: 22.08.2017].

[16] uBlox, "Datasheet: Neo-7p u-blox 7 precise point positioning gnss module," accessed online 25.07.2017. [Online]. Available: https://www.u-blox.com/sites/default/files/products/documents/NEO-7P_DataSheet_\%28UBX-13003787\%29.pdf

[17] T. I. Fossen, *Handbook of Marine Craft Hydrodynamics and Motion Control*. Wiley, 2011.

[18] J. M. Hovem, "Underwater acoustics: Propagation, devices and systems," *Journal of Electroceramics*, vol. 19, no. 4, pp. 339–347, 2007. [Online]. Available: https://doi.org/10.1007/s10832-007-9059-9

[19] Hovem, Jens. M, *Marine acoustics : the physics of sound in underwater environments*. Los Altos Hills, Calif: Peninsula Publishing, 2012.

[20] F. Gustafsson, *Statistical sensor fusion*, 2nd ed. Lund: Studentlitteratur, 2012.

[21] P. D. Groves, *Principles of GNSS, inertial, and multi-sensor integrated navigation systems*. Boston/ London: Artech House, 2008.

[22] R. E. Kalman and R. S. Bucy, "New results in linear filtering and prediction theory," *Journal of basic engineering*, vol. 83, pp. 95–108, 1961. [Online]. Available: internal-pdf://246.154.102.32/95_1.pdfLB-kalmanBucy

[23] R. G. Brown and P. Y. C. Hwang, *Introduction to Random Signals and Applied Kalman Filtering with Matlab Exercises, 4th Edition*, ser. Introduction to random signals and applied Kalman filtering. John Wiley and Sons, 2012.

[24] R. E. Walpole, R. H. Myers, S. L. Myers, and K. Ye, *Probability and Statistics for Engineers and Scientists*. Pearson Education Limited, 2012, vol. 3rd.

[25] R. A. Johnson and D. W. Wichern, *Applied Multivariate Statistical Analysis*, 6th ed. Pearson Prenctice Hall, 2007.

[26] S. S. Sandøy and I. Schjølberg, "Experimental verification of underwater positioning system in aquaculture," in *OCEANS 2017 - Aberdeen*, Conference Proceedings, pp. 1–7.